Surfactant Stabilized Bubbles Flowing in a Newtonian Fluid

Eilis Rosenbaum*, Mehrdad Massoudi†, Kaushik Dayal‡

*‡Department of Civil and Environmental Engineering, Carnegie Mellon University

*†National Energy Technology Laboratory

‡Center for Nonlinear Analysis, Carnegie Mellon University

‡Department of Materials Science and Engineering, Carnegie Mellon University

May 16, 2019

Abstract

Bubbles suspended in a fluid cause the suspension to have different rheological properties than the base fluid. Generally, the viscosity of the suspension increases as the volume fraction of the bubbles is increased. A current application, and motivation for this study, is in wellbore cements used for hydrocarbon extraction and carbon sequestration. In these settings, the gas bubbles are dispersed into the cement to reduce the density as well as improve the properties for specific conditions or wellbore issues. In this paper, we use Stokesian dynamics to numerically simulate the behavior of a large number of bubbles suspended in a Newtonian fluid. Going beyond prior work on simulating particles in suspension, we account for the nature of bubbles by allowing for slip on the bubble surface, the deflection on the bubble surface, and a bubble-bubble pairwise interaction that represents the surfactant physics; we do not account for bubble compressibility. We incorporate these interactions and simulate bubble suspensions of monodisperse size at several volume fractions. We find that the bubbles remain better dispersed compared to hard spherical particles that show a greater tendency to structure or cluster.

Keywords: Stokesian Dynamics, dense suspension, foamed cement, rheology, bubble suspension.

1 Introduction

The motivation for this study is to better understand the rheology of well cement that has been foamed with an inert gas. Foaming the cement lowers the density, and is used in wells drilled

*Email: Eilis.Rosenbaum@netl.doe.gov
†Email: Mehrdad.Massoudi@netl.doe.gov
‡Email: Kaushik.Dayal@cmu.edu

into weak or fractured rock formations [1]. Foamed cement is created by dispersing gas, typically nitrogen, into the cement slurry to create a suspension, which contains suspended cement particles, and dispersed bubbles. To ensure a stable foam that keeps the bubbles entrained, surfactants and sometimes other additives are included in the slurry base prior to injecting the gas to form the bubbles. In the wellbore, cement is placed between the steel casing at the center of the well and the rock formation to isolate and seal wells in carbon storage and hydrocarbon extraction. It also supports the casing placed in the center of the well. The process of foaming the cement slurry lowers the density of the cement as required for the conditions of the wellbore. Foaming the cement is advantageous because it lowers the density and increases the viscosity of the cement, while not significantly lowering the compressive strength nor changing the cement chemistry. To maintain isolation of the well, however, the bubbles should remain suspended in the cement and maintain dispersion. Structuring or clustering can lead to weak mechanical regions for crack propagation or pathways for gas migration.

Cement slurry is a highly complex material with properties that change over time due to the curing process. The cement slurry (base fluid) is made from water that is mixed with the cement clinker, a powdery mix of materials with primarily lime, silica, alumina, and iron. Upon mixing with water, the chemical reaction processes begin in the form of a hydration process [2]. During the hydration process the chemical and the physical properties of the cement slurry are changing. However, the cement does have a period when little hydration occurs and this is when the cement is placed in the wellbore. During this *induction* period, the slurry properties remain fairly constant and the effect of chemical reactions can be neglected. The behavior is dominated by fluid mechanics. A key focus of this paper is the effect of the flow on the overall ordering of the bubbles that are added through foaming. There is a vast literature on the effective properties of suspensions, e.g. going back to Taylor, 1932 [3]; for more information see [4]. There is much less work on the structuring of the suspended bubbles.

The bubbles' distribution within the cement play a key role in the properties of the cement slurry [5]. The foam should have well-dispersed bubbles, that remain in the suspension during placement without clustering, coalescing, or other configurations where the bubbles are arranged closely together [1]. If the bubbles are close to each other, upon curing the bubbles can become interconnected and lead to failure of zonal isolation or even fracture of the cement [6, 7]. The American Petroleum Institute (API) recommended practices prescribes that the foamed cement slurries be designed to have an added gas volume fraction below 35% at the placement depth of the cement for the foam to remain stable and maintain the mechanical integrity for proper zonal isolation [8]. Pressures vary throughout the cement process due to different depths in the well; we, therefore, study a range of volume fractions (10% to 50%).

In [9], we studied the influence of the bubbles represented as hard no-slip spheres using the framework of Stokesian Dynamics [10] in the more efficient Fast Lubrication Dynamics (FLD) approximation [11–13]. This method enables us to track the location of all the suspended objects during the simulation, and thereby obtain insights into smaller scale phenomena such as the detailed spatial distribution. An important assumption that is required for Stokesian Dynamics is that the base fluid is Newtonian. Our aim in this paper is to develop better representations of the bubbles while working within this overall framework to include far- and near-range bubble interactions. In particular, we account for the nature of bubbles by allowing for slip on the bubble surface, the deflection

on the bubble surface at the region where bubble pairs interact, and a bubble-bubble pairwise interaction that represents the surfactant physics, which can be attractive or repulsive in nature [14]. For simplicity, in this paper *particles* shall refer to hard spherical particles that have no-slip boundary conditions on their surface; and *bubbles* shall refer to fluid-filled spheres with surface properties that allow slip and surface deflection in the interacting region, and a repulsive/attractive quality to represent the surfactant properties, but however are not compressible.

The paper is organized as follows: in Section 2, we outline our assumptions and briefly describe the well-established Stokesian Dynamics framework and the FLD approximation; in Section 3, we provide the details of the bubble interaction modeling; in Section 4, we describe the molecular dynamics simulation method; in Section 5, we present the results of the numerical calculations on the relative viscosity of the bubble suspension; and in Section 6, we present the results of the numerical calculations comparing bubble suspensions to the rigid no-slip particle suspensions studied in [9] and examine several volume fractions with monodisperse size distributions.

2 Model Assumptions and the Stokesian Dynamics Method

2.1 Model Assumptions

We make several assumptions about the bubbles and the system of interest.

The bubbles are assumed to be spherical and discrete. Surfactants are an essential part of the cement slurry design and the surfactant provides stability to the bubbles so that they remain suspended in the cement until is sets [5]. Bubbles stabilized by surfactants have a high surface tension and maintain a relatively spherical shape. It is assumed that the bubbles have and maintain a spherical shape during flow and are not distorted or become ellipsoid-like during shearing. Foamed cements made in the laboratory to the API testing standards and foamed under pressure show that the surfactants and stabilizers added to the base fluid maintain fairly spherical, stable, discrete bubbles in the flow regime typically encountered in the well [15, 16]. However, the bubble surface is allowed to deflect locally on the surface a small amount in the region directly interacting with neighboring bubbles.

The bubbles are considered to be neutrally buoyant. In an aqueous solution, bubbles will rise due to buoyancy. However, in a stable foamed cement slurry, bubbles in cement tend to remain in place unless they reach a critical size [16]. This has been observed experimentally [15–17]: in laboratory and field applications, the bubble sizes are kept below this critical size (typically around $10 - 100$ μm) and were observed to remain where placed during curing [16]. In addition, the cement particles in the slurry, which act as surface active foaming materials, help keep the bubbles entrained [18].

The suspending fluid (cement slurry) is considered Newtonian. The cement slurry has cement particles suspended in it, and therefore it is generally observed that cement slurry has a yield stress and can behave as a nonlinear fluid [19, 20], or even behave as a solid [21]. However, it would not be feasible to numerically simulate a non-Newtonian suspension that tracks individual bubbles. We therefore expect that the simulation results reported here will have qualitative and quantitative differences compared to experiments. Even so, these simulations can provide useful insights into

the overall features that dictate the behavior of the real system, specifically the clustering of bubbles or rearrangement into more ordered placements which can potentially lead to bubble coalescence or bubble inter-connectivity upon cement curing. For simulations involving one or a small number of bubbles, sophisticated nonlinear models of the suspending medium can be applied [22]. However, for a large number of suspended objects as is our interest here, the methods depend in an essential way on the superposition principle and hence require linearity.

2.2 Stokesian Dynamics

In a suspension, the motion of each suspended object (particles or bubbles) is transmitted through the base fluid. In the quasi-static (creeping flow) limit, this is felt immediately throughout the entire system by all the other suspended objects. Therefore long-range effects should be carefully considered. For a dilute suspension where the suspended objects are far apart, the detailed shape and structure of the suspended objects does not matter to leading-order. The velocity disturbance of a suspended object decays like a point force as $1/r^2$, where r is the radial distance from the object [10]. When the suspended objects are close together, the interaction of each pair is dominated by a pairwise force which comes from lubrication theory [23]. The Stokesian Dynamics method accounts for the far-field interaction through multipole expansions and for the near-field interactions through pairwise interactions [10]. The Fast Lubrication Dynamics (FLD) method further increases the efficiency by using fast approximate methods for the far-field interaction [11, 12]. The broader idea of developing multiscale methods for long-range interactions by decomposing into far- and near- fields and then using multipole expansions for the far-field has been studied theoretically and numerically in the context of bubbly fluids [24] and electromagnetic interactions [25–27].

For the flow of a Newtonian fluid when the inertial term is neglected in the balance of linear momentum, we can obtain the Stokes flow regime. The governing equation is a linear biharmonic equation, thereby allowing superposition. Given a flow with multiple objects, the flow due to each is given by a fundamental solution denoted by a Stokeslet, and the interaction between them can be obtained by superposing appropriately the Stokeslets solutions. This enables an *effective* pairwise interaction where the influence of the mediating fluid is accounted through the Stokeslet. Bossis and Brady were the first to develop this idea and put this into the framework of pairwise molecular dynamics to enable the efficient simulation of suspensions [10, 28]. This method is denoted "Stokesian Dynamics".

Consider a general macroscopically-uniform flow $\boldsymbol{v}(\boldsymbol{x}) = \boldsymbol{A}\cdot\boldsymbol{x}+\boldsymbol{B}$, where $\boldsymbol{x}$ is the spatial location. The symmetric rate-of-strain tensor is defined $\boldsymbol{E}^\infty := \frac{1}{2}(\boldsymbol{A}+\boldsymbol{A}^T)$, where $\boldsymbol{A}$ is the velocity gradient. The spin tensor is defined by $\boldsymbol{W} := \frac{1}{2}(\boldsymbol{A}-\boldsymbol{A}^T)$ and the corresponding axial vector is $\boldsymbol{w}$. The generalized far-field velocity $\boldsymbol{U}^\infty$ is defined by $\boldsymbol{B}$ and $\boldsymbol{w}$. The forces can be determined by the relationship between the object velocities and the forces due to the base fluid by:

$$\begin{pmatrix} \boldsymbol{F}^H \\ \boldsymbol{S}^H \end{pmatrix} = \mathcal{R} \cdot \begin{pmatrix} \boldsymbol{U}^\infty - \boldsymbol{U} \\ \boldsymbol{E}^\infty \end{pmatrix} \tag{2.1}$$

The symmetric first moment of the force, $\boldsymbol{S}^H$, is called the Stresslet. $\mathcal{R}$ is the resistance matrix, and contains the object positions. The main outcome of Stokesian Dynamics is to efficiently compute

$\mathcal{R}$ so that large numbers of objects in a suspension can be simulated. This is described in numerous sources in the literature cited in this manusript, and therefore, we do not go into the details here.

Stokesian Dynamics preserves all the relevant physics of the problem but is computationally intense for systems with a large number of suspended objects. To allow for larger systems while still maintaining the physics of the problem in accounting properly for far-field and near-field interactions, *Fast Lubrication Dynamics* (FLD) was developed [11, 12].

FLD [11, 12] explicitly incorporates the lubrication interactions, following [29], but modifies the Stokesian Dynamics [10] to reduce the computation time. In FLD, the resistance matrix, denoted $\mathcal{R}_{FLD}$, is the sum of the near-field pairwise lubrication interactions and the far-field interactions from the diagonal components of an isotropic resistance tensor, $\mathcal{R}_{Iso}$. $\mathcal{R}_{Iso}$ is assumed to be a multiple of the identity matrix. The multiplicative factor is assumed to be a function of the volume fraction, and is obtained by curve-fitting the short-time self-diffusivity results from FLD to those obtained from full Stokesian Dynamics. In this way, FLD aims to preserve the physics of the accurate Stokesian Dynamics approach while making the computation more efficient. The lubrication terms come from [23, 29, 30].

We note an issue regarding the implementation of FLD in the molecular dynamics code LAMMPS. [29] give the expressions for the lubrication forces and torques of each suspended object in the pair interaction. However, LAMMPS uses truncated expressions that leave out some terms. FLD in LAMMPS has typically been applied in combination with other forces such as Brownian, colloidal, electrostatic, and so on. The error due to the missing terms can be negligible if other interactions dominate. However, for the calculations here, we find that it is important to use the longer expressions, and therefore we have corrected LAMMPS.

3 Bubble Interaction Modeling

Our approach is to simulate fluid-filled spheres of the same diameter with bubble surface properties and an elastic-like quality. For the purposes of this study, we consider that the bubbles have hydrodynamic interactions and some interaction due to the properties of a surfactant to keep bubbles from overlapping in the simulation. The attractive and repulsive qualities of the surfactant are also considered with this interaction. The bubbles' surfaces are allowed to deform locally in an elastic way when approaching very close to each other (see Figure 5, and then the bubble surface shape is restored when the gap between the bubble pair increases, so that the spherical bubble shape is maintained during the simulation.

The hydrodynamic interaction for a pair of bubbles, with the same size diameter, has been derived by [23] for the case of two bubbles of the same size approaching each other. The interaction due to the surfactant and elastic properties are determined and added here. For approaching hard spheres with no slip on the particle surface, the force between the particles goes as the inverse of the gap between them, so that as the particles approach each other, the force increases so much so that the particles will not touch in finite time. The force on approaching bubbles is weaker and will allow bubbles to touch in finite time. In simulations, without an additional direct force, bubble overlap will occur. However, the surfactant of real bubbles will provide an extra force that resists bubble

coalescence. The force between the bubbles should be such that it does not allow bubbles to overlap but does allow them to approach very close to each other.

Bubbles have a mobile interface and, in theory, can have any level of slip and no shear traction on their surface boundaries. In a shearing interaction between bubble pairs, the bubbles should just slip past each other [23, 31]. To simulate surfactant stabilized bubbles, we need to have a mobile surface boundary and an additional realistic normal direct force to prevent bubble overlap as the surfactant does in real bubble suspensions.

Bubble surface properties more representative of real bubbles stabilized by a surfactant has been developed here as an extension to the current capabilities of LAMMPS pair interactions.

3.1 Summary of Near-Field Lubrication Interactions for Particles

We briefly summarize the near-field interactions between particles to later compare to bubble interactions.

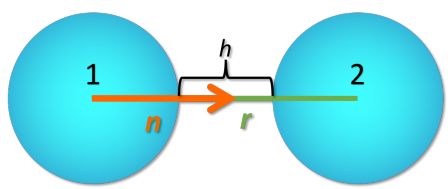

Figure 1: Two particles are separated by a center-to-center vector, $\boldsymbol{r}$, and $\boldsymbol{n} := \boldsymbol{r}/|\boldsymbol{r}|$. The gap between the particles is h.

Following Fig. 1, we consider a pair of particles 1 and 2, with equal radius, a, and a separation h between the particle surfaces. The expressions for the lubrication forces $\boldsymbol{f}_i$ and torques $\boldsymbol{g}_i$ on the particles $i = 1, 2$ follows [29]:

$$\boldsymbol{f}_1 = -\boldsymbol{f}_2 = -a_{sq}\mathbb{N}\cdot(\boldsymbol{v}_1 - \boldsymbol{v}_2) - a_{sh}\left(\frac{2}{r}\right)^2 \mathbb{P}\cdot(\boldsymbol{v}_1 - \boldsymbol{v}_2) + \left(\frac{2}{r}\right) a_{sh}\boldsymbol{n}\times\mathbb{P}\cdot(\boldsymbol{\omega}_1 + \boldsymbol{\omega}_2) \quad (3.1a)$$

$$\boldsymbol{g}_1 = -\left(\frac{2}{r}\right) a_{sh}\boldsymbol{n}\times\mathbb{P}\cdot(\boldsymbol{v}_1 - \boldsymbol{v}_2) - a_{sh}\mathbb{P}\cdot(\boldsymbol{\omega}_1 + \boldsymbol{\omega}_2) - a_{pu}\mathbb{P}\cdot(\boldsymbol{\omega}_1 - \boldsymbol{\omega}_2) - a_{tw}\mathbb{N}\cdot(\boldsymbol{\omega}_1 - \boldsymbol{\omega}_2) \quad (3.1b)$$

$$\boldsymbol{g}_2 = -\left(\frac{2}{r}\right) a_{sh}\boldsymbol{n}\times\mathbb{P}\cdot(\boldsymbol{v}_1 - \boldsymbol{v}_2) - a_{sh}\mathbb{P}\cdot(\boldsymbol{\omega}_1 + \boldsymbol{\omega}_2) + a_{pu}\mathbb{P}\cdot(\boldsymbol{\omega}_1 - \boldsymbol{\omega}_2) + a_{tw}\mathbb{N}\cdot(\boldsymbol{\omega}_1 - \boldsymbol{\omega}_2) \quad (3.1c)$$

$\boldsymbol{n}$ is the unit vector directed along the line connecting the center of particle 1 pointing toward particle 2, $\mathbb{N} := \boldsymbol{n}\otimes\boldsymbol{n}$, and $\mathbb{P} := \boldsymbol{I} - \mathbb{N}$. $\boldsymbol{v}$ and $\boldsymbol{\omega}$ are the velocity and the angular velocity, respectively, of the particles. The forces $\boldsymbol{f}$ and torques $\boldsymbol{g}$ in (3.1) correspond to the generalized force and are linearly related to $\boldsymbol{v}$ and $\boldsymbol{\omega}$, and these latter quantities in turn correspond to the generalized velocity $\boldsymbol{U}$. The linear resistance terms for hard spheres of differnt sizes with no-slip surfaces, a_{sq}, a_{sh}, a_{pu}, and a_{tw}, are defined in [9].

For bubbles, there is a squeezing resistance, a_{sq}, but it is assumed that there are no shearing resistances (i.e. $a_{sh} = 0$ and $a_{pu} = 0$). The hydrodynamic forces for a bubble are still linearly related to the velocity and the force is calculated in a similar way as the lubrication solution for hard sphere [9] (Equations (3.1)). The force between bubbles includes additional forces to account for the elastic nature of a bubble and the forces due to the surfactant.

3.2 Near-Field Bubble Interactions: Interaction Force Between Approaching Bubbles

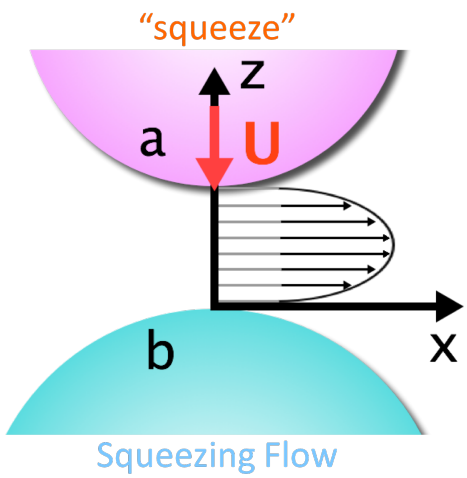

Figure 2: The surface of bubbles have slip and therefore the velocity profile contains an additional slip velocity (shown in gray).

The interaction force between approaching hard spheres with no-slip surfaces is sufficient to keep the particles from touching in finite time. But for two approaching bubbles, they will touch in finite time and can overlap. Figure 4 compares the gap as a function of time for particles and bubbles, without accounting for surface deflection of the latter. The velocity profile of a Newtonian fluid being squeezed from between the hard spheres has a parabolic shape. However, a bubble surface boundary has an extra slip velocity as depicted in Figure 2. The velocity profile of the fluid between the interacting bubbles is the sum of the parabolic velocity, u_p, and the additional slip velocity, u_t, due to the bubble surface [23, 32]:

$$v(x, z) = u_t(x) + u_p(x, z) \tag{3.2}$$

The parabolic velocity profile of the fluid that is squeezed out from between hard spheres with no-slip boundaries is given by the expression [23]:

$$u_p(x, z) = \frac{1}{2\mu}\frac{\partial p}{\partial x}(z - z_a)(z - z_b) \tag{3.3}$$

Where z_a and z_b are the surfaces of the two spheres a and b, respectively, μ is the viscosity of the base fluid, and $\frac{\partial p}{\partial x}$ is the pressure gradient in the x direction. When the distance between the bubble

surfaces is small compared to the bubble radii, the surfaces can be approximated as flat disks and the surface traction is then given by [23]:

$$f_t = -(z_a - z_b)\frac{\partial p}{\partial x} \tag{3.4}$$

If μ is the viscosity of the base fluid, then by convention $\lambda\mu$ is defined as the viscosity of the bubble. For a bubble, $\lambda = 0$. The traction boundary condition at the base fluid - bubble interface is [23]:

$$\mu\frac{\partial u_p}{\partial z} = \lambda\mu\frac{\partial v}{\partial z} \tag{3.5}$$

The solution for two bubbles with equal diameters has been derived in bispherical coordinates by [23].

The relationship between the force and velocity for approaching bubbles and squeezing flow is [23]:

$$\frac{F_i}{6\pi\mu a U_i} = \frac{1}{3}\log\frac{a}{h} + \frac{2}{3}(\gamma_{Euler} + \log 2) + O(1) \tag{3.6}$$

where γ_{Euler} is Euler's constant (γ_{Euler} = 0.577216...), a is the radius of the bubble, and h is the gap between the bubbles. This can then be rearranged to solve for the force, F_i, as a function of velocity, U_i, so that the remaining terms on the right become the resistance "squeeze" coefficient for a bubble, which is used instead of the a_{sq} coefficient derived by Ball and Melrose [29]. The force of bubble i is then:

$$F_i^{Bubble} = 6\pi\mu a U_i\left(\frac{1}{3}\log\frac{a}{h} + \frac{2}{3}\left(\gamma_{Euler} + \log 2\right)\right) \tag{3.7}$$

Equation (3.7) describes the normal force acting on bubble i, and therefore a_{sq}^{Bubble} is given by:

$$a_{sq}^{Bubble} = \pi\mu a\left(2\log\frac{a}{h} + 4\left(\gamma_{Euler} + \log 2\right)\right) \tag{3.8}$$

Using this squeeze coefficient, for two bubbles being pushed together with an equal and opposite external force, the gap between their surfaces can be described as a function of time (Fig. 4).

The leading term for the squeezing flow between hard spheres with no-slip surfaces is $1/h$, and for bubbles it is $\log 1/h$. To look at the effects of this difference, we consider two particles being pushed together by applying an external force in equal and opposite directions to each particle. According to the lubrication theory [23], hard spherical particles with no slip surfaces should not touch in finite time. In this squeezing flow, only the squeeze term is involved in the interaction, as the velocities of the particles are acting normal to the surface of the particles. The gap as a function of time with an external force of $f_x = 1$, we define by:

$$\frac{dh}{dt} = \frac{1}{-a_{sq}} \tag{3.9}$$

We define the total time by the integral, $I_{a_{sq}} := \int dt = -\int a_{sq} dh$. For hard spheres with no-slip boundary conditions:

$$I_{a_{sq}} = \frac{27h\pi}{40} + \frac{9h^2\pi}{224} + \frac{27}{40}h\pi\log\frac{1}{2h} + \frac{9}{112}h^2\log\frac{1}{2h} + \frac{3}{8}\pi\log h \tag{3.10}$$

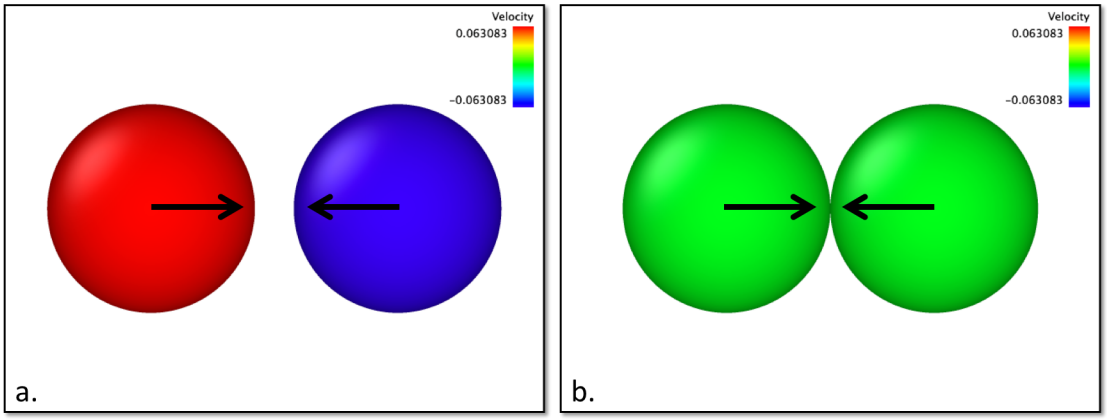

Figure 3: Two hard spherical particles, with no-slip surfaces, of equal size (diameter $= 1$) are being pushed together. a.) The starting positions of the particles. Their initial velocities in the horizontal direction is shown by their color. b.) At the end of the simulation, with constant external force pushing equally in opposite directions, the particles will approach very close to each other but should not touch in finite time.

For a bubble with slip boundary conditions:

$$I_{a_{sq}}^{Bubble} = 2\pi h + 4\gamma_{Euler}\pi h + 2\pi h \log 4 + 2\pi h \log \frac{1}{h} \tag{3.11}$$

Define $h_0 = h(t = 0)$. This gives:

$$t = I_{a_{sq}}(h_0) - I_{a_{sq}}(h) \tag{3.12}$$

The gap as a function of time using Equation (3.12) compares the lubrication interactions of two hard sphere particles with no-slip surfaces and two spherical bubbles with slip surfaces approaching each other due to equal and opposite forces ($f_x = \pm 1$) acting on each particle/bubble (Figure 4). The diameter, d, was set to 1 for both particles/bubbles.

Figure 3 shows the velocity at the beginning and end of the simulations for hard spheres. The hard spheres with no-slip surfaces should not touch in finite time. Figure 3 also shows the particle positions relative to each other and the arrows indicate the motion of the particles approaching each other. The velocity of the particles at the beginning and end of the short simulation are indicated by the color of the particles. Initially, the particle velocities are equal and opposite due to the linear relationship with the forces on the particles. At the end of the simulation, the external force remains the same on each particle but the velocity approaches zero as the particles approach very close to each other and the gap becomes nearly zero. But, due to the high lubrication forces, the particle surfaces will not touch in finite time.

Figure 4 shows the gap from Figure 3 as a function of time. The hard spherical particles will come very close to each other but the high force due to the fluid between them will prevent them from touching in finite time. For bubbles, however, the force is weaker and the bubbles will overlap in finite time. In implementing this into simulations, for hard spheres with no slip boundaries, a

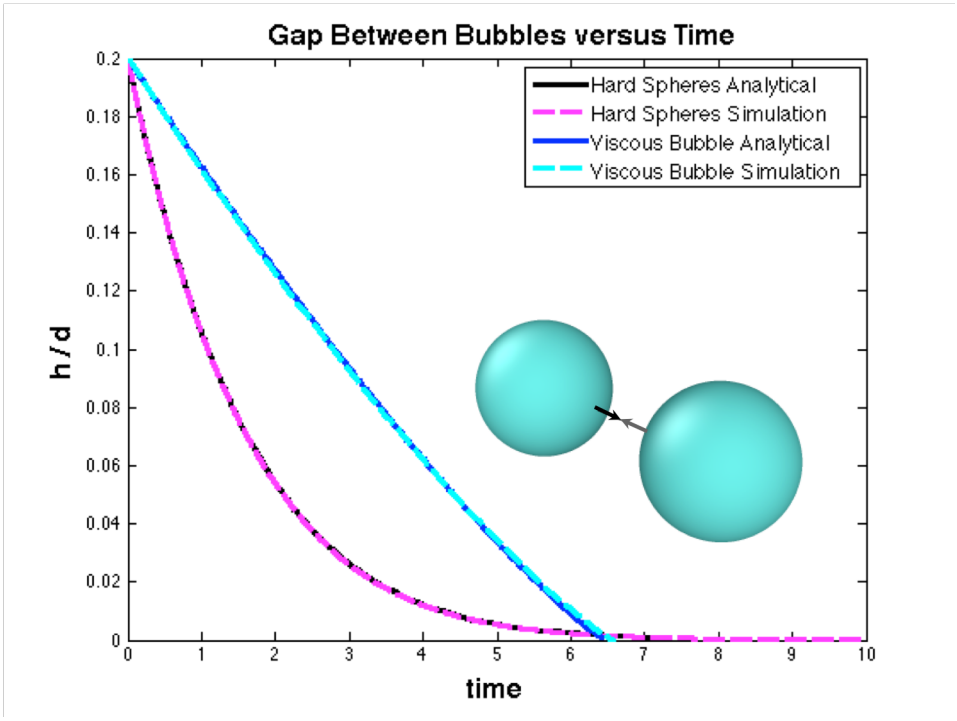

Figure 4: Gap between the approaching particles/bubbles as a function of time. Comparison between hard spheres with no-slip on the surfaces (black $-$, magenta $--$) with bubbles with slip on the surfaces (viscous bubble, blue $-$, cyan $--$).

cutoff distance is used for the interactions. If the particle gap is less than the cutoff, the cutoff is used in place of the actual gap to calculate the forces and torques. Otherwise, the particles could overlap during the simulation. Another approach would be to make the timestep smaller and smaller to avoid overlaps [29]. For bubbles, especially at higher volume fractions where the bubbles interact more, as the suspension is sheared, the bubbles can overlap in an unphysical way. To keep the bubbles from overlapping completely, a direct force, $\boldsymbol{F}^{Direct}$, is also necessary. A real bubble surface is also not rigid so to account for this property, an elastic-like force, $\boldsymbol{F}^{Elastic}$, is also included. The total normal force on the bubble surface between interacting pairs is therefore described by:

$$\boldsymbol{F}^{Total} = \boldsymbol{F}^{Bubble} + \boldsymbol{F}^{Elastic} + \boldsymbol{F}^{Direct} \tag{3.13}$$

$\boldsymbol{F}^{Bubble}$ is defined by Equation (3.7). We next describe the elastic and direct forces, $\boldsymbol{F}^{Elastic}$ and $\boldsymbol{F}^{Direct}$, respectively.

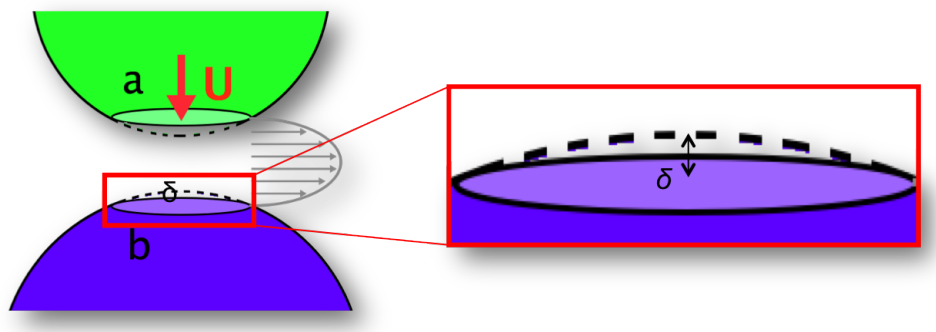

Figure 5: The bubble surface can deflect by an amount, δ.

3.3 Near-Field Bubble Interactions: Elastic Force

As noted above, an elastic force is required to model the distortions away from spherical of the bubble due to the impingement of another bubble. The elastic force derivation follows [33]:

$$\boldsymbol{F}^{Elastic} = a_{Elas} E \delta \tag{3.14a}$$

$$a_{Elas} = \sqrt{a(2h + |\delta|)} \tag{3.14b}$$

$$\delta = \frac{(2a + h - r)}{2} \tag{3.14c}$$

Here, δ is the deflection of the bubble surface(Figure 5), a_{Elas} is the region of the bubble surface that is interacting in the lubrication force after deflection has caused the surface to become flattened, and E represents an *effective* modulus to deform the interface and bubble. In the simulations shown here, E was set to 10^2; this could in principle be calibrated to experiment. To limit the amount that the bubble surface can deflect, a maximum deflection value was set.

3.4 Near-Field Bubble Interactions: Direct Force

The direct force is necessary to keep the bubbles from overlapping during the simulation. It represents the force due to the surfactant, which can be attractive and repulsive [14] depending on the properties of the surfactant and the separation of the bubbles. The surfactant forces can include van der Waals and hydrostatic attraction, electrostatic repulsion, steric repulsion, etc. [14], however, the properties of the surfactant are not the focus of this research and are not generally known as they are proprietary. Therefore, no specific surfactant will be considered. Herein, the direct force is represented by a Lennard-Jones potential force that acts normal to the bubble surface along the line between the center of interacting bubble pairs. Rognon and Gay [34, 35] developed soft dynamics

to simulate dense collections of elastic particles. Soft dynamics can only simulate closely interacting particles and a confining stress is used to keep the suspension in a dense configuration. Rognon, Einav, and Gay [33, 36] include a direct force that represents the steric repulsion between elastic particles. It increases steeply when the particles come in close contact and prevents the particles from overlapping. In the simulations shown here, a direct force is deployed in a similar way. The Lennard-Jones potential included with LAMMPS [37] was used as the direct force.

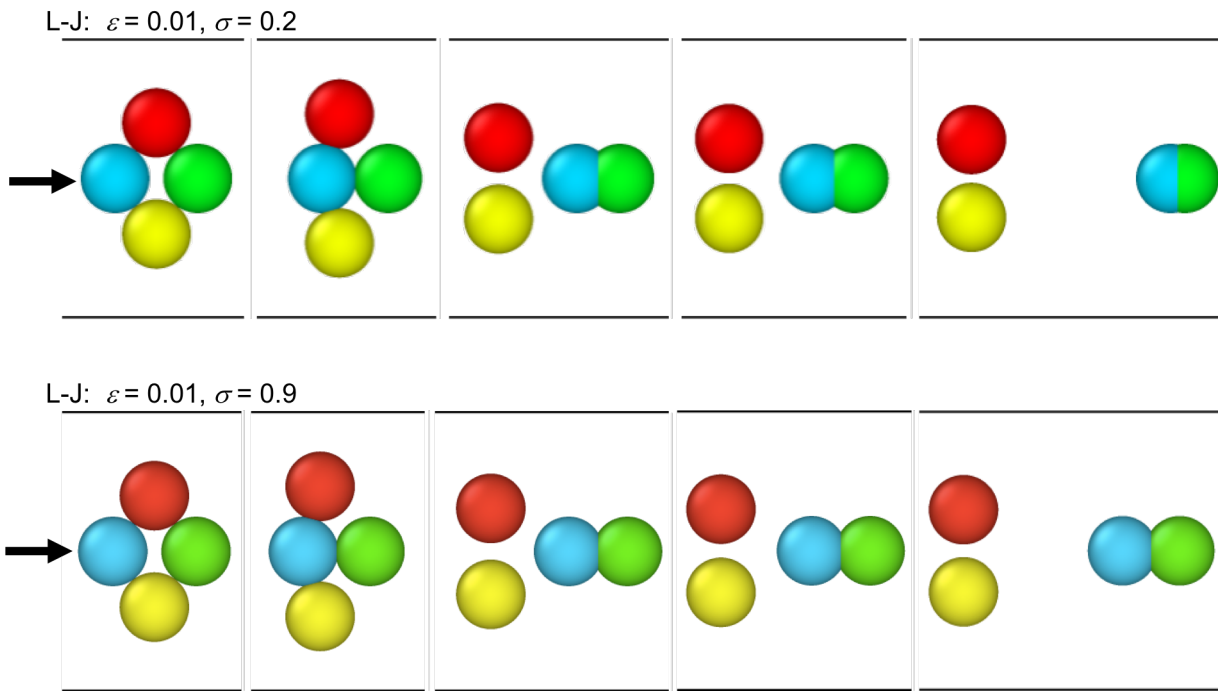

Figure 6: Simple four-bubble configurations were used to explore the influence of the ϵ and σ values of the Lennard-Jones potential. The force is applied to the bubble indicated by the arrow in the first time frame. The configuration changes of the bubbles are displayed over a several time steps. The left most frame is the starting configuration and the right most frame shows the center bubbles at their limit of deflection due to the force applied. The combination of the ϵ and σ values dictate the level that bubbles are allowed to deflect and the level of attraction of the bubbles. The bubble force and the elastic force are also included in the interaction.

The Lennard-Jones potential is based on van der Waals interactions [33, 36] and includes both repulsive and attractive forces. A Lennard-Jones potential that was less repulsive than the standard Lennard-Jones potential was used here and is given by [37]:

$$\phi_{LJ} = 4\epsilon \left[\left(\frac{\sigma}{r}\right)^9 - \left(\frac{\sigma}{r}\right)^6 \right] \tag{3.15}$$

ϵ is the energy scale and σ is the length scale. The influence of the values of ϵ and σ on systems dynamics are described below. $\left(\frac{\sigma}{r}\right)^9$ is the repulsive part[1] and $\left(\frac{\sigma}{r}\right)^6$ is the attractive portion. The

[1]The standard Lennard-Jones potential is $\phi_{LJ} = 4\epsilon \left[\left(\frac{\sigma}{r}\right)^{12} - \left(\frac{\sigma}{r}\right)^6 \right]$

direct force, F^{Direct}, between bubbles is then the derivative of Equation (3.15). Here, this force keeps the bubbles from overlapping completely but also allows for the elastic interaction.

3.5 The Lennard-Jones Parameters for the Direct Force

The values for ϵ and σ can be varied to adjust: (1) the amount that the bubbles' surface can deflect, and (2) the level of attraction between the bubbles. To test the influence of ϵ and σ, four bubble configurations were used. A constant force of 1 was applied to the left most bubble and the images shown in Figure 7 show a snapshot in time of the simulation after the left-most bubble has started interacting with the other bubbles. Periodic boundary conditions were used so that once the center bubbles passed through the top and bottom bubbles, they were remapped into the simulation box on the left side. As the simulations progressed, the amount of deflection and attraction between the bubbles was observed.

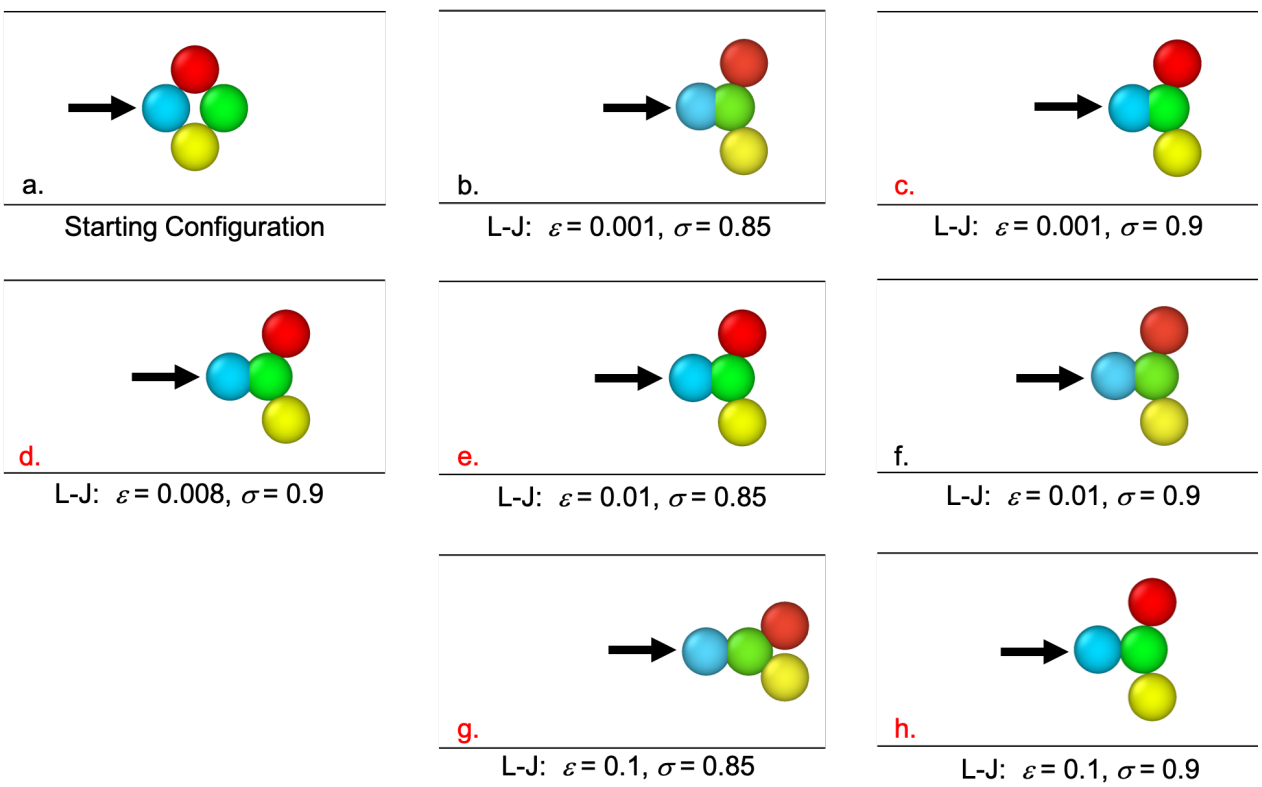

Figure 7: Simple four-bubble configurations were used to explore the influence of the ϵ and σ values of the Lennard-Jones potential. The bubble direct force and the elastic force are included in the interaction. a.) Shows the starting configuration of the bubbles. The arrow shows where the force is applied. A force was only applied to the bubble indicated. b.), c.), d.), e.), f.), g.) and h.) show the influence of changing the values of ϵ and σ.

Figure 6 shows the progression of the bubble configurations over several time steps. If the values of ϵ and σ are not chosen correctly, then the bubbles can overlap too much and do not represent the

system dynamics properly. Values of $\epsilon = 0.01$ and $\sigma = 0.2$ allow too much overlap (deflection) of the bubbles in an unrealistic manner. Another observation is that the top and the bottom bubbles move close to each other and almost touch. The combination of ϵ and σ also dictate the amount of attraction between the bubbles. The lower the value of σ – which sets the length scale of the interaction – the greater the overlap, for a given value of ϵ. Figure 7 shows the influence of several parameter combinations. Figure 7a. shows the initial configuration of the bubbles. The lower the value of ϵ, the greater the overlap, but the slightly lower value of σ causes the bubbles to be more attractive and have a "softening" effect. In Figure 7g, as the force continues to push the left most bubble, the bubbles in the middle were also pushed because they were attracted to each other similar to what is observed in Figure 6a. The combination of the higher energy and length scale, are shown in Figure 7h. The combination of the Lennard-Jones potential $\epsilon = 0.1$ and $\sigma = 0.9$ values, result in a direct force that does not allow the bubble surface to deflect. Effectively, the bubbles then act like hard spheres.

The Lennard-Jones potential is being utilized as the direct force representing the surfactant properties, which means that it must have the proper level of repulsion to keep the bubbles from completely overlapping but also some attraction to represent the surfactant. Five combinations of ϵ and σ were considered to determine the values that best represent the physical properties of the bubbles. Figures 7c., d., e., g., and h. show the combinations that were simulated with full system sizes.

Figure 7c. corresponds to $\epsilon = 0.001$ and $\sigma = 0.9$, which allows the bubbles to deflect sufficiently but the attraction, though not pictured here, is high enough that the top and bottom bubbles approach close to each other when the center bubbles pass through. Lennard-Jones values of $\epsilon = 0.01$ and $\sigma = 0.85$ (Figure 7e.) resulted in similar results as the combination of $\epsilon = 0.001$ and $\sigma = 0.9$. For the values of $\epsilon = 0.1$ and $\sigma = 0.85$ (Figure 7g.), the top and bottom bubbles touch after the center bubbles pass through. Figure 8a. shows the time progression of the bubbles' motion from Figure 7g. As the left-most bubble is pushing on the other bubbles, the deflection of the surface appears to be reasonable but when the center bubbles are pushed through the top and bottom bubbles, the top and bottom bubbles are excessively attracted to each other. For values of $\epsilon = 0.1$ and $\sigma = 0.9$ (Figure 7h. and Figure 8b.), the physics of the problem are similar to hard spheres. The bubbles can still slip by each other with no resistance tangent to the bubble surface but the higher σ value did not allow deflection of the bubbles' surface so the results mimic those of hard spheres. So even without a shearing resistance in the interaction, the behavior of the bubbles is similar to hard spherical particles. The best combination of values was $\epsilon = 0.008$ and $\sigma = 0.9$ (Figure 7d.), which allowed some deflection of the bubble surface and some attraction.

4 Molecular Dynamics Simulation Method

LAMMPS[2] – the Large-scale Atomic/Molecular Massively Parallel Simulator – is an open-source classical (non-quantum) molecular dynamics code developed and maintained at Sandia National Labs [38]. We use LAMMPS with the FLD method[3] combined with bubble surface properties.

[2] lammps.sandia.gov

[3] As noted previously, we have extended LAMMPS to include bubble-like surface properties in the resistance terms.

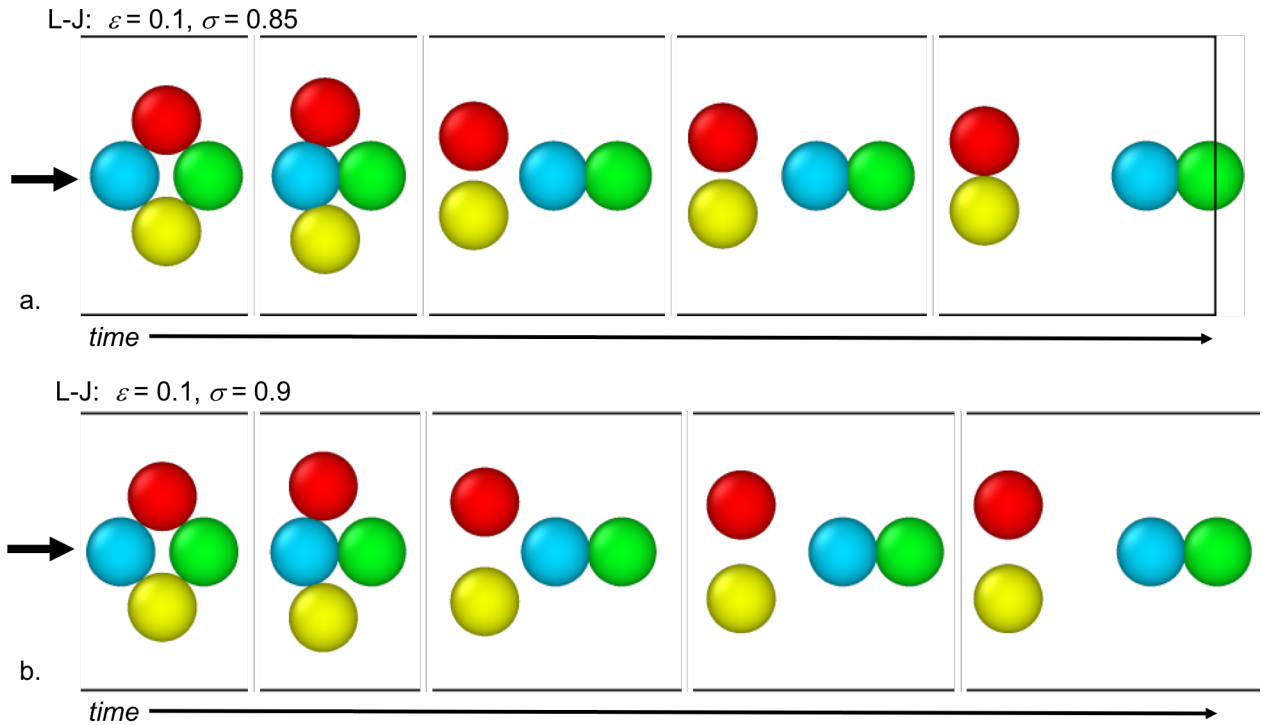

Figure 8: The configuration changes of the bubbles are displayed over a several time steps. a.) Corresponds to Figure 11e. and b.) Corresponds to Figure 11f. The force is applied to the bubble shown by the arrow in the first time frame. The left most frame is the starting configuration and the right most frame shows the center bubbles at their limit of deflection due to the force applied. The combination of the ϵ and σ values dictate the level that bubbles are allowed to deflect and the level of attraction of the bubbles. The bubble force and elastic force are also included in the interaction.

4.1 Generation of Initial Configurations of Bubbles

Bubble systems were generated by first creating smaller sets in a $10 \times 10 \times 10$ box. The bubbles with a diameter of 1 were randomly placed to create different volume fractions (10%, 20%, 30%, 40%, 45%, and 50%) of bubbles all having the same system volume. Once the bubbles are randomly placed, a soft potential is used with an energy minimization to remove overlaps in the initial configuration that are unphysical[4]. The energy of the soft potential is [37]:

$$E = A\left(1 + \cos\left(\frac{\pi r}{r_{cut}}\right)\right), \quad r < r_{cut} \tag{4.1}$$

where r is the distance between bubbles, A is the pre-factor in energy units that was initially set low and ramped up, and r_{cut} is the cut off distance.

To avoid effects from the system size, testing was done to determine the appropriate system size that shows no further size dependence. The system sizes were progressively doubled in all coordinate

[4]We emphasize that the soft potential is used only in generating a physical initial configuration, and plays no role once the simulation begins.

directions until an appropriate size, where the system size did not impact the calculation of the relative viscosity, was achieved. It was determined that replicating the original system size of $10 \times 10 \times 10$ four times in each direction eliminated system size effects. Once this configuration was replicated, the bubbles were then moved around using the random Brownian pair interaction in LAMMPS to make the bubble arrangements random again. This step was not part of the dynamics but was simply to create a random placement of the bubbles after replicating the same arrangement of bubbles, for input into the simulations.

4.2 Implementation of the Shearing Flow

The shearing flow was implemented as described in [9]. Three dimensional simulations were performed using Lees-Edwards boundary conditions [39]. For Lees-Edwards boundary conditions and strains imposed in the xy-direction, the velocity of each bubble is then a function of its position in the y-direction as shown in Figure 9. When a bubble crosses the simulation boundary in any direction, the velocity of the bubble is remapped to correspond to the new position in the simulation box[5]. The suspensions of different volume fractions were all sheared as shown in Figure 9 until the stress reached a constant value and the value of $\dot{\gamma} \times t_{total}$ reached 200. t_{total} is the length of time that the simulation was run and $\dot{\gamma} \times t_{total}$ was used so that all simulations results were comparable. Basically, all simulations were run till the box was sheared the same amount as opposed to being run for the same length of time. Testing different time steps revealed that the dimensionless time step should be kept below a value of 0.002 for the FLD simulations, however, a timestep of $\Delta t = 0.001$ was used for all simulations shown here. An explicit time-integration scheme was used.

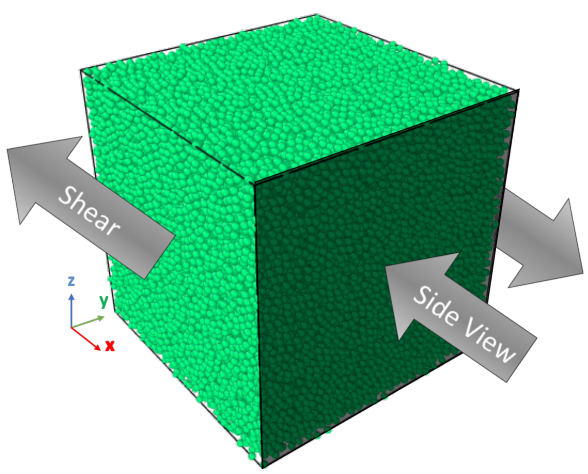

Figure 9: The bubble suspensions are sheared in the direction shown and when the side view is shown, it is a view through the whole system of bubbles.

The total strain on the simulation box is defined as $\dot{\gamma} \times \Delta t$, the product of the strain rate $\dot{\gamma}$ and timestep Δt. For the quasi-static setting, given $\dot{\gamma} \times \Delta t$, the time-history of the stress and viscosity

[5] See e.g. [40] for a discussion of this and [37] for the implementation, which uses a function called "fix deform" to apply a strain rate to the simulation box in the specified orthogonal box directions.

should be the same when time is appropriately re-scaled.

The stress in the system is calculated by summing the stresses computed for each bubble. Ignoring the kinetic energy contributions that are negligible here, the stress on a bubble is defined by [37,41]:

$$\sigma_{i,\alpha\theta} = \frac{1}{V_i}[-\frac{1}{2}\sum_{n=1}^{N_p}(r_{1_\alpha}F_{1_\theta} + r_{2_\alpha}F_{2_\theta})] \tag{4.2}$$

where, α and θ run over the coordinate directions to compute the 6 components of the symmetric stress tensor. The sum runs over the N_p neighbors of the bubble under consideration. $\boldsymbol{r}_1$ and $\boldsymbol{r}_2$ are the positions of every bubble pair that has pairwise interactions, and $\boldsymbol{F}_1$ and $\boldsymbol{F}_2$ are the corresponding forces.

For a simulation box with volume, V, the stress from each bubble is summed to determine the total stress of the system of bubbles and is used to calculate the viscosity. With Lees-Edwards boundary conditions imposed, the relative viscosity (i.e., the viscosity ratio) is calculated from the average total stress once the system has reached steady state:

$$\mu_{\text{relative}} = \frac{\mu_{\text{effective}}}{\mu} = \frac{\sum_i \sigma_{xy}}{\dot{\gamma}\mu V} \tag{4.3}$$

5 Viscosity Ratio of the Bubble Suspension

An important reason to add bubbles to a fluid is to increase the effective viscosity. In this section, we examine the effect of the bubble volume fraction on the viscosity based on the molecular dynamics calculations.

Recall the definition of the viscosity ratio in Equation (4.3). The viscosity ratio as a function of bubble volume fraction is shown in Figure 10. The initial configurations were all the same for comparison of the effects of the Lennard-Jones parameters ϵ and σ values on the viscosity. As described above, the choice of $\epsilon = 0.1$ and $\sigma = 0.85$ did not display proper system dynamics and the relative viscosity calculated was significantly higher than the other simulations, which is also unrealistic. The choice of $\epsilon = 0.1$ and $\sigma = 0.9$ produced physics that were not characteristic of bubbles and the relative viscosity values are also unrealistic as described above.

The combination of the ϵ and σ values influence the level of bubble deflection and the level of attraction. The level of deflection and the level of attraction between the bubbles ultimately influences the distance between bubbles and the force between bubble pairs, which is used to compute the stress on each bubble. The effect of ϵ and σ are shown in Figure 7c., d., e., g., and h. for the relative viscosity values displayed in Figure 10a. The relative viscosity is dependent on the stress in the system, which is a summation of the stresses on each bubble. Figure 11 shows the value of stress in the xy-direction, $\sigma_{i,xy}$, for each bubble at the final configuration of the simulation. Figure 11a shows the stress per bubble at the beginning of the simulation. The results are only shown for the 0.50 bubble volume fraction suspensions because the close-range interactions that were developed here are the most dominant in dense suspensions. Figure 11e., corresponding to the choice of $\epsilon = 0.1$ and $\sigma = 0.85$, shows an overall higher stress on each bubble – when compared to the other

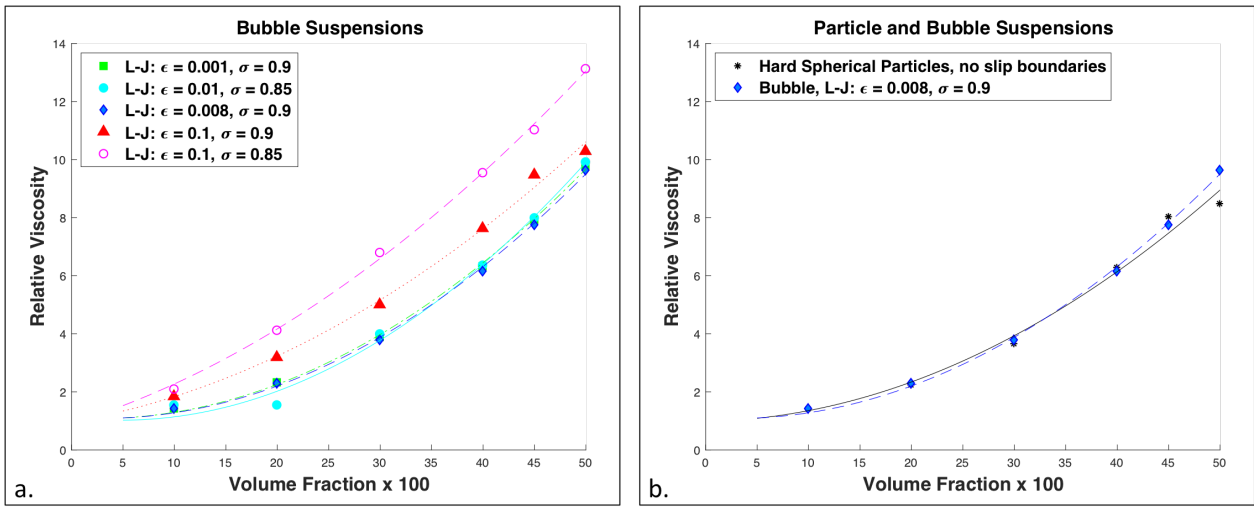

Figure 10: The relative viscosity or viscosity ratio is shown as a function of the volume fraction of bubbles in the suspension. The lines in the figures are second order polynomial fits through the calculated relative viscosity points shown and including the point $(0, 1)$ a.) The influence of ϵ and σ of the Lennard-Jones direct force in the bubble interaction are shown. b.) Hard sphere suspension results [9] are compared with the results of bubble suspensions.

simulation results shown – which results in higher viscosity values than when the other Lennard-Jones parameters are used. The choice of $\epsilon = 0.1$ and $\sigma = 0.85$ does not produce reasonable relative viscosity results and the problem dynamics are not physically realistic either as shown in 7g.

The final choice of $\epsilon = 0.008$ and $\sigma = 0.9$ of the Lennard-Jones parameters were chosen based on allowing the bubbles to overlap slightly but also have only a small amount of attraction to represent the effects of the surfactant. The bubble properties described from this point further will assume to have $\epsilon = 0.008$ and $\sigma = 0.9$ values for the Lennard-Jones potential. The bubble configurations used as inputs for the simulation results shown here are the same as those used for monodisperse hard spheres with no slip boundary conditions [9]. The viscosity ratio of monodisperse hard spheres with no-slip boundaries are shown in Figure 10b, for comparison to the viscosity calculated for bubbles with slip boundaries and the ability to deform elastically in the manner described in Section 3. With the parameters chosen for these simulations, the viscosity ratio of bubble suspensions – as modeled here – does not vary an appreciable amount from the viscosity ratio of monodisperse hard sphere suspensions.

6 Structuring of Suspensions of Bubbles v. Particles

As discussed above, the structuring or clustering of bubbles in suspension can lead to weak mechanical regions for crack propagation or pathways for gas migration. In this section, we compare monodisperse bubble suspensions to monodisperse particle suspensions using molecular dynamics

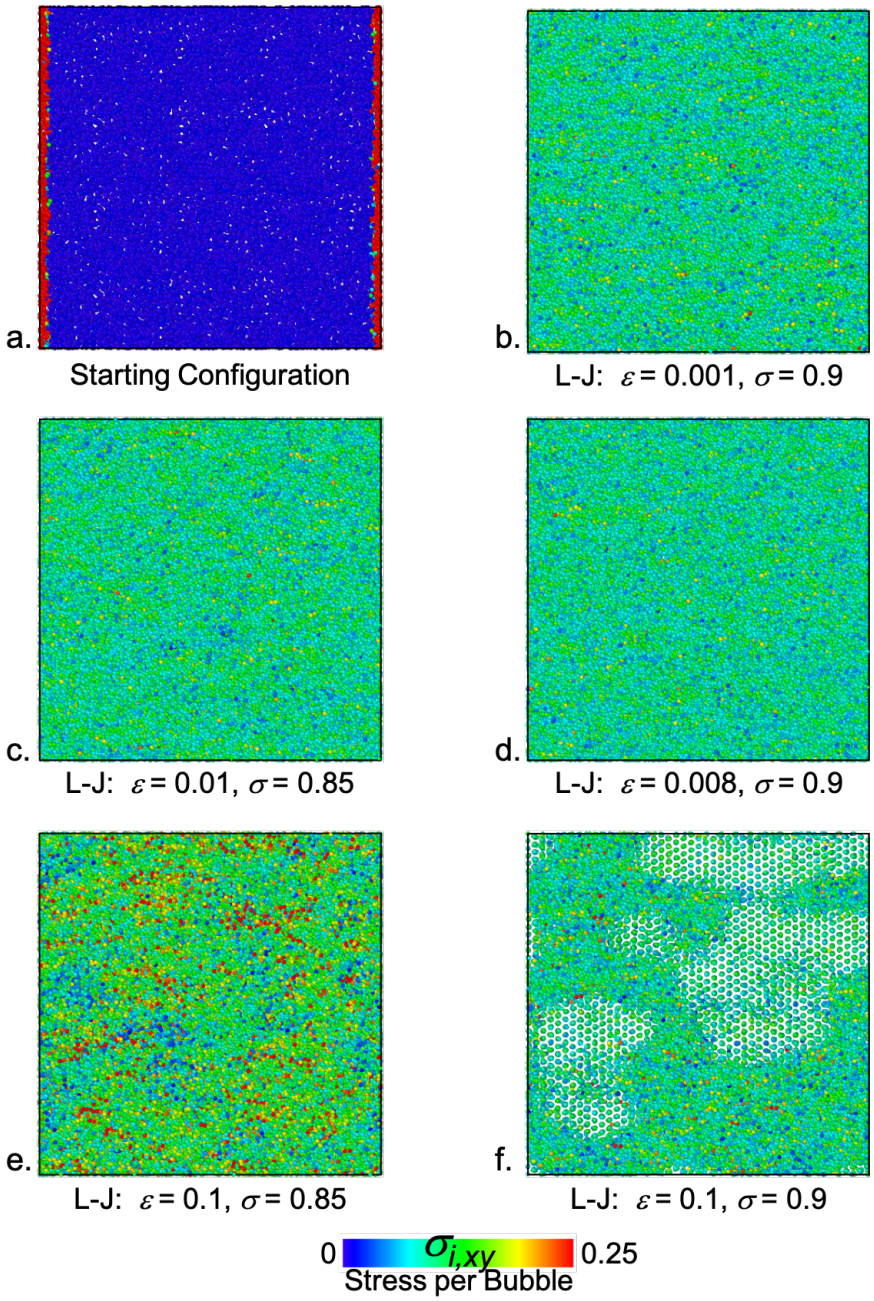

Figure 11: The final configuration of the 0.50 volume fraction of bubbles is shown in b.), c.), d.), e.), f.) and the initial configuration of the bubbles and stress per bubble is shown in a.). The color of each bubble corresponds to the value of the stress per bubble (from Equation (4.2)). The bubbles are shown at half size and form the view shown in Figure 9.

calculations.

Using parameters in the simulations that maintain proper system dynamics, the numerical simulations show that the relative viscosity calculated is not influenced a significant amount by the

properties of the bubble surface compared to hard sphere particle suspensions. Figure 12 compares monodisperse particles to monodisperse bubbles. The stress per particle/bubble is indicated by color. The input configurations are the same for comparison and only the 0.50 volume fraction is compared because it is the higher volume fraction where detrimental clustering or ordering [9]. The resulting relative viscosity is the same for both particles and bubbles but the per particle stress varies more in the hard sphere particles. Because the summation of the stress results in similar total average stress, the relative viscosity is also similar for both particles and bubbles.

The difference in the surface properties of particles versus bubbles affects the spatial arrangement. The monodisperse particles have a lubrication squeezing force that prevents them from touching. The hard spheres also have shearing resistance. The properties of monodisperse particle suspensions was explored previously [9], and it was shown that volume fractions of 0.47 and higher show rearrangement and ordering. Monodisperse hard spherical particles, with no-slip boundary conditions, in a suspension will go from a random placement to an ordered placement that locally resembles a crystalline packing. Figure 13 compares the qualitative results of monodisperse particles to monodisperse bubbles. In Figure 13b, the re-arrangement and structuring of the particles can be observed. In Figure 13a, the alignment of the particles can also be seen in the form of chains of particles. However, the influence of the bubble surface properties keep the bubbles relatively well dispersed throughout the simulation. Figures 13c and d show the results of the bubble suspensions described here. Unlike the hard spheres, the bubbles have a softer force between them, no shearing resistance due to the slip surface, and a surface that is able to deflect. The effects of the bubble surface properties help to keep the bubbles dispersed and the same ordering of particles seen in Figure 13b is not observed in Figure 13d.

In Figure 13, the correlation refers to the pair correlation function of each bubble. The pair correlation quantifies the number of neighboring bubbles in volumetric shells (of equal thickness) around each bubble. The pair correlation of each bubble was calculated using the expression:

$$g(\eta) = \frac{N_S}{\frac{N}{V} V_S} \tag{6.1}$$

N_S is the number of bubbles in the current shell, S. V_S is the volume of the current shell and $\frac{N}{V}$ is the number density of bubbles in the whole simulation box. The pair correlation values of the particles/bubbles, shown in Figure 13, is the probability of finding neighboring particles/bubbles within a spherical radius, η, of 1.5 away from each particle/bubble. The pair correlation relates to the ordering of the particles/bubbles. The hard sphere suspensions that show ordering of the particles have a higher correlation value for the particles in those regions. The bubble suspensions maintain an overall lower level of correlation. The level of correlation of the bubbles is consistent throughout the whole simulation box.

7 Discussion

Due to the slip on the bubble surface, lack of shearing resistance, and by allowing the bubble surface to deflect a small amount, interacting bubble pairs can pass by each other with less restriction. This results in less jamming of the bubbles, which is what causes bubbles to start forming linear

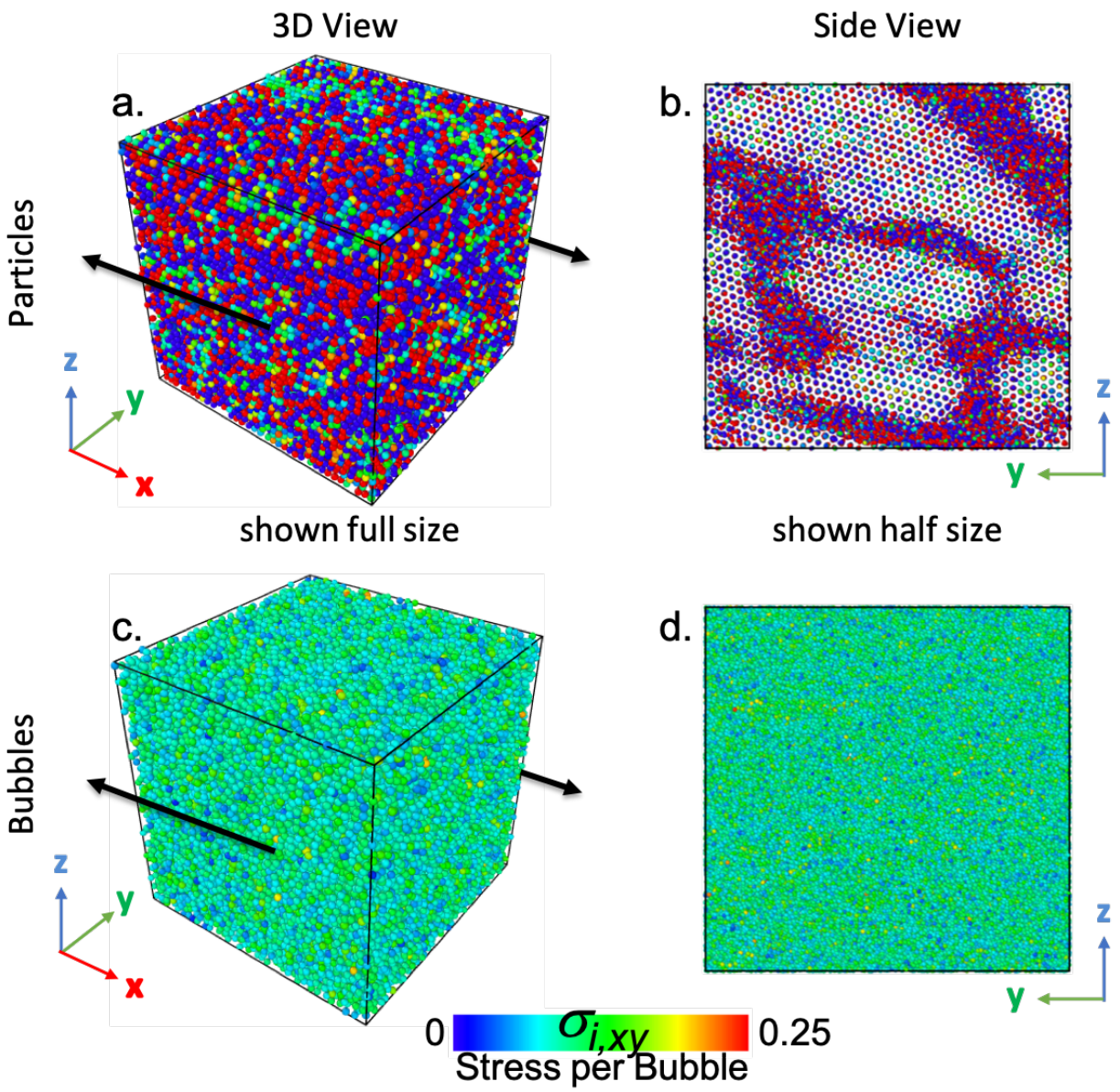

Figure 12: The final configuration of 0.50 volume fraction of particles/bubbles simulations is shown. Particles are compared to the bubbles. For the bubble results shown, the values of the Lennard-Jones potential are $\epsilon = 0.008$ and $\sigma = 0.9$.

structures (Figure 12b.). With application to foamed cements, it is desired to keep the bubbles dispersed throughout the cement slurry, during placement in the well and once placed. As shown in [9], the effect of the particle polydispersity is to reduce clustering. Also, monodisperse bubbles structure and cluster less when compared to monodisperse particles.

One of the benefits of foaming the cement is the increase in the viscosity. The increased viscosity with the amount of added bubbles enhances the drilling mud removal [42], especially in the type

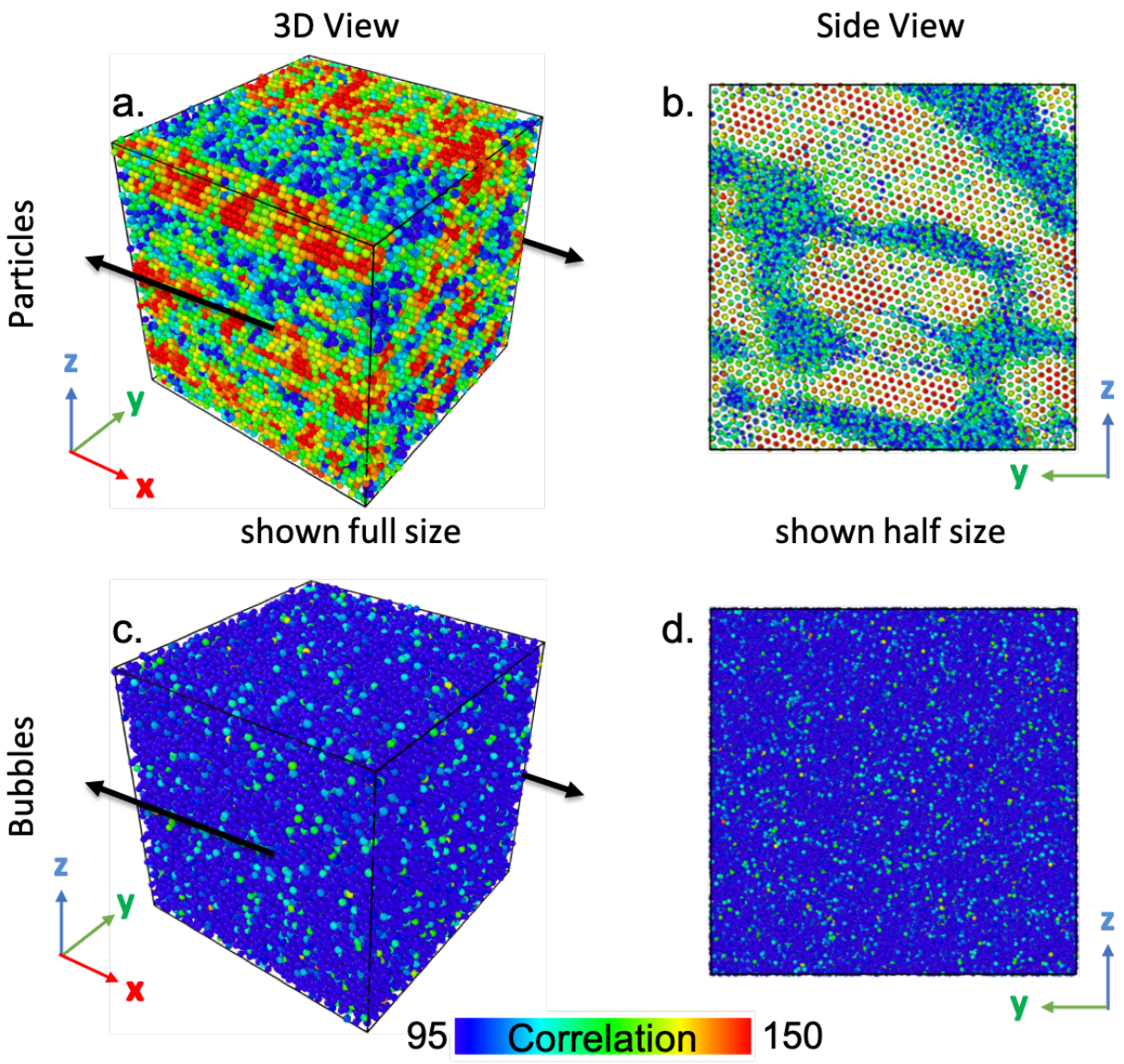

Figure 13: The final configuration of 0.50 volume fraction of particles/bubbles simulations is shown. Particles are compared to bubbles. For the bubble results shown, the values of the Lennard-Jones potential are $\epsilon = 0.008$ and $\sigma = 0.9$.

of mud used in geothermal wells [43]. Our numerical calculations show that in both particle and bubble suspensions, the viscosity increases with the increase in volume fraction of suspending objects [44].

It is expected – and will be explored in the future – that the combination of bubble surface properties with polydispersity in the bubbles sizes would further reduce the propensity for bubble clustering to occur. In application, it is difficult to create bubble dispersions of exactly equal bubbles so in actual foamed cement, the polydispersity of the bubbles in the foamed cement help to keep the bubbles

dispersed. However, simulations with polydisperse bubble sizes is a significant step beyond the monodisperse modeling presented here, and is an important goal for the future.

The calculations here assume Newtonian suspending fluids, which is a limitation of the overall Stokesian Dynamics framework. Homogenization or mixture-theory based approaches, e.g. based on [4, 45–53], may enable the formulation of continuum models that can provide insight into particle structuring while also accounting for the complex rheology of cement paste.

Acknowledgments

Kaushik Dayal acknowledges an appointment to the National Energy Technology Laboratory Faculty Research Participation Program sponsored by the U.S. Department of Energy and administered by the Oak Ridge Institute for Science and Education.

Declaration of Conflicting Interests

The authors declare that there is no conflict of interest.

Funding

Computing resources were provided by the National Science Foundation through the Extreme Science and Engineering Discovery Environment (XSEDE) program; specifically the XSEDE Bridges Computing Resources at the Pittsburgh Supercomputing Center [grant number TG-DMR160018]. Kaushik Dayal was supported through an appointment to the National Energy Technology Laboratory Faculty Research Participation Program sponsored by the U.S. Department of Energy and administered by the Oak Ridge Institute for Science and Education.

Research Data

The LAMMPS simulation code is available publicly at `lammps.sandia.gov`. Our implementation within the LAMMPS framework of the interactions described in this paper are publicly available at `github.com/eilisjill/Pair_style_bubble`.

Disclaimer

References

[1] N. Loeffler, "Foamed Cement: A Second Generation," in *Permian Basin Oil and Gas Recovery Conference*, 1984.

[2] J. de Rozieres and T. J. Griffin, "Chapter 14 Foamed Cements," in *Well Cementing* (E. B. Nelson, ed.), pp. 14.1 – 14.19, Schlumberger Educational Services, 300 Schlumberger Drive, Sugar Land, Texas 77478, 1990.

[3] G. I. Taylor, "The viscosity of a fluid containing small drops of another fluid," *Proceedings of the Royal Society of London. Series A, Containing Papers of a Mathematical and Physical Character*, vol. 138, no. 834, pp. 41–48, 1932.

[4] M. Massoudi, "A note on the meaning of mixture viscosity using the classical continuum theories of mixtures," *International Journal of Engineering Science*, vol. 46, no. 7, pp. 677–689, 2008.

[5] J. de Rozières and R. Ferrière, "Foamed-Cement Characterization Under Downhole Conditions and Its Impact on Job Design," *SPE Production Engineering*, no. August, pp. 297–304, 1991.

[6] L. Tan, G. Ye, E. Schlangen, and K. Van Breugel, "Coupling of hydration and fracture models: Failure mechanisms in hydrating cement particle systems," *Particle and Continuum Aspects of Mesomechanics*, pp. 563–571, 2007.

[7] L. K. Tan, E. Schlangen, and G. Ye, "Simulation of failure in hydrating cement particles systems," *Key Engineering Materials*, vol. 348, pp. 737–740, 2007.

[8] American Petroleum Institute, "Isolating Potential Flow Zones During Well Construction - API Standard 65 Part 2," 2010.

[9] E. Rosenbaum, M. Massoudi, and K. Dayal, "Effects of polydispersity on structuring and rheology in flowing suspensions," *To appear in Journal of Applied Mechanics*, 2019.

[10] J. F. Brady and G. Bossis, "Stokesian dynamics," *Annual review of fluid mechanics*, vol. 20, no. 1, pp. 111–157, 1988.

[11] M. D. Bybee, *Hydrodynamic Simulations of Colloidal Gels: Microstructure, Dynamics, and Rheology*. PhD thesis, University of Illinois at Urbana-Champaign, 2009.

[12] A. Kumar, *Microscale Dynamics in Suspensions of Non-Spherical Particles*. PhD thesis, University of Illinois at Urbana-Champaign, 2010.

[13] A. Kumar and J. J. L. Higdon, "Origins of the anomalous stress behavior in charged colloidal suspensions under shear," *Physical Review E - Statistical, Nonlinear, and Soft Matter Physics*, vol. 82, no. September, pp. 1–7, 2010.

[14] S. S. Tabakova and K. D. Danov, "Effect of disjoining pressure on the drainage and relaxation dynamics of liquid films with mobile interfaces," *Journal of Colloid and Interface Science*, vol. 336, no. 1, pp. 273–284, 2009.

[15] B. Kutchko, D. Crandall, M. Gill, D. McIntyre, R. Spaulding, B. Strazisar, E. Rosenbaum, I. Haljasmaa, G. Benge, E. Cunningham, G. DeBruijn, and C. Gardner, "Computed Tomography and Statistical Analysis of Bubble Size Distributions in Atmospheric-Generated Foamed Cement," Tech. Rep. August, 2013.

[16] L. E. Dalton, S. Brown, J. Moore, D. Crandall, and M. Gill, "Evolution Using CT Scanning : Insights From Elevated-Pressure Generation," no. January, pp. 1–11, 2018.

[17] B. Kutchko, D. Crandall, J. Moore, M. Gill, D. McIntyre, E. Rosenbaum, I. Haljasmaa, B. Strazisar, R. Spaulding, W. Harbert, G. Benge, E. Cunningham, D. W. Lawrence, G. DeBruijn, and C. Gardner, "Field-generated foamed cement: Initial collection, computed tomography, and analysis," tech. rep., U.S. Department of Energy, National Energy Technology Laboratory, 2015.

[18] R. J. Pugh, "Foaming, foam films, antifoaming and defoaming," *Advances in Colloid and Interface Science*, vol. 64, no. 95, pp. 67–142, 1996.

[19] N. Roussel, "Steady and transient flow behaviour of fresh cement pastes," *Cement and Concrete Research*, vol. 35, pp. 1656–1664, 2005.

[20] D. Guillot, "Rheology of Well Cement Slurries," *Developments in Petroleum Science*, vol. 28, no. C, pp. 4–1–4–37, 1990.

[21] A. Beltempo, M. Zingales, O. S. Bursi, and L. Deseri, "A fractional-order model for aging materials: An application to concrete," *International Journal of Solids and Structures*, vol. 138, pp. 13–23, 2018.

[22] R. Gaudron, M. Warnez, and E. Johnsen, "Bubble dynamics in a viscoelastic medium with nonlinear elasticity," *Journal of Fluid Mechanics*, vol. 766, pp. 54–75, 2015.

[23] S. Kim and S. J. Karrila, *Microhydrodynamics: Principles and Selected Applications*. Mineola, NY: Dover Publications, Inc., 2nd ed., 2005.

[24] A. Sangani and A. Acrivos, "The effective conductivity of a periodic array of spheres," *Proc. R. Soc. Lond. A*, vol. 386, no. 1791, pp. 263–275, 1983.

[25] R. D. James and S. Müller, "Internal variables and fine-scale oscillations in micromagnetics," *Continuum Mechanics and Thermodynamics*, vol. 6, no. 4, pp. 291–336, 1994.

[26] Y. Xiao, *The influence of oxygen vacancies on domain patterns in ferroelectric perovskites*. PhD thesis, California Institute of Technology, 2005.

[27] J. Marshall and K. Dayal, "Atomistic-to-continuum multiscale modeling with long-range electrostatic interactions in ionic solids," *Journal of the Mechanics and Physics of Solids*, vol. 62, pp. 137–162, 2014.

[28] G. Bossis and J. F. Brady, "Dynamic simulations of sheared suspensions. {I.} General method," *J. Chem. Phys.*, vol. 80, no. 10, pp. 5141–5154, 1984.

[29] R. C. Ball and J. R. Melrose, "A simulation technique for many spheres in quasi-static motion under frame-invariant pair drag and Brownian forces," *Physica A: Statistical Mechanics and its Applications*, vol. 247, no. 1-4, pp. 444–472, 1997.

[30] D. J. Jeffrey and Y. Onishi, "Calculation of the resistance and mobility functions for two unequal rigid spheres in low-Reynolds-number flow," *Journal of Fluid Mechanics*, vol. 139, no. -1, p. 261, 1984.

[31] C. Bechinger, F. Sciortino, and P. Ziherl, *Physics of Complex Colloids*. IOS Press, 2013.

[32] R. H. Davis, J. a. Schonberg, and J. M. Rallison, "The lubrication force between two viscous drops," vol. 77, no. 1989, 1989.

[33] P. G. Rognon, I. Einav, and C. Gay, "Internal relaxation time in immersed particulate materials," *Physical Review E - Statistical, Nonlinear, and Soft Matter Physics*, vol. 81, no. 6, pp. 1–9, 2010.

[34] P. G. Rognon and C. Gay, "Soft Dynamics simulation. 1. Normal approach of two deformable particles in a viscous fluid and optimal-approach strategy," *European Physical Journal E*, vol. 27, pp. 253–260, 2008.

[35] P. G. Rognon and C. Gay, "Soft dynamics simulation. 2. Elastic spheres undergoing a T 1 process in a viscous fluid," *European Physical Journal E*, vol. 30, pp. 291–301, 2009.

[36] P. G. Rognon, I. Einav, and C. Gay, "Flowing resistance and dilatancy of dense suspensions: lubrication and repulsion," *Journal of Fluid Mechanics*, vol. 689, pp. 75–96, 2011.

[37] *LAMMPS Users Manual*. Sandia National Laboratories, 2003.

[38] S. Plimpton, "Fast Parallel Algorithms for Short – Range Molecular Dynamics," *Journal of Computational Physics*, vol. 117, no. June 1994, pp. 1–19, 1995.

[39] A. Lees and S. Edwards, "The computer study of transport processes under extreme conditions," *Journal of Physics C: Solid State Physics*, vol. 5, no. 15, p. 1921, 1972.

[40] K. Dayal and R. D. James, "Nonequilibrium molecular dynamics for bulk materials and nanostructures," *Journal of the Mechanics and Physics of Solids*, vol. 58, no. 2, pp. 145–163, 2010.

[41] E. B. Tadmor and R. E. Miller, *Modeling materials: continuum, atomistic and multiscale techniques*. Cambridge University Press, 2011.

[42] G. J. Frisch, H. E. Services, and W. L. Graham, "SPE 55649 Assessment of Foamed - Cement Slurries Using Conventional Cement Evaluation Logs and Improved Interpretation Methods," *SPE Rocky Mountain Regional Meeting*, 1999.

[43] D. Bour and B. Rickard, "Application of Foamed Cement on Hawaiian Geothermal Well," *Geothermal Resources Council Transactions*, vol. 24, 2000.

[44] G. Batchelor and J. Green, "The determination of the bulk stress in a suspension of spherical particles to order c 2," *Journal of Fluid Mechanics*, vol. 56, no. 3, pp. 401–427, 1972.

[45] R. Lipton and M. Avellaneda, "Darcy's law for slow viscous flow past a stationary array of bubbles," *Proceedings of the Royal Society of Edinburgh Section A: Mathematics*, vol. 114, no. 1-2, pp. 71–79, 1990.

[46] R. Lipton and B. Vernescu, "Homogenisation of two-phase emulsions," *Proceedings of the Royal Society of Edinburgh Section A: Mathematics*, vol. 124, no. 6, pp. 1119–1134, 1994.

[47] T. Gao, H. H. Hu, and P. P. Castañeda, "Shape dynamics and rheology of soft elastic particles in a shear flow," *Physical review letters*, vol. 108, no. 5, p. 058302, 2012.

[48] T. Gao, H. H. Hu, and P. P. Castañeda, "Rheology of a suspension of elastic particles in a viscous shear flow," *Journal of Fluid Mechanics*, vol. 687, pp. 209–237, 2011.

[49] R. Avazmohammadi and P. P. Castañeda, "Macroscopic rheological behavior of suspensions of soft solid particles in yield stress fluids," *Journal of Non-Newtonian Fluid Mechanics*, vol. 234, pp. 139–161, 2016.

[50] J. Christoffersen, M. Mehrabadi, and S. Nemat-Nasser, "A micromechanical description of granular material behavior," *Journal of applied mechanics*, vol. 48, no. 2, pp. 339–344, 1981.

[51] M. Massoudi, "On the importance of material frame-indifference and lift forces in multiphase flows," *Chemical Engineering Science*, vol. 57, no. 17, pp. 3687–3701, 2002.

[52] M. Massoudi, "Constitutive relations for the interaction force in multicomponent particulate flows," *International Journal of Non-Linear Mechanics*, vol. 38, no. 3, pp. 313–336, 2003.

[53] M. Massoudi, "A mixture theory formulation for hydraulic or pneumatic transport of solid particles," *International Journal of Engineering Science*, vol. 48, no. 11, pp. 1440–1461, 2010.